Stress modulation on the San Andreas fault by interseismic fault system interactions

John P. Loveless* and Brendan J. Meade
Department of Earth and Planetary Sciences, Harvard University, Cambridge, Massachusetts 02138, USA

ABSTRACT

During the interseismic phase of the earthquake cycle, between large earthquakes, stress on faults evolves in response to elastic strain accumulation driven by tectonic plate motions. Because earthquake cycle processes induce non-local stress changes, the interseismic stress accumulation rate on one fault is influenced by the behavior of all nearby faults. Using a geodetically constrained block model, we show that the total interseismic elastic strain field generated by fault interactions within Southern California may increase stressing rates on the Mojave and San Bernardino sections of the San Andreas fault within the Big Bend region by as much as 38% relative to estimates from isolated San Andreas models. Assuming steady fault system behavior since the C.E. 1857 Fort Tejon earthquake, shear stress accumulated on these sections due only to interaction with faults other than the San Andreas reaches 1 MPa, ~3 times larger than the coseismic and postseismic stress changes induced by recent Southern California earthquakes. Stress increases along Big Bend sections coincide with the greatest earthquake frequency inferred from a 1500-yr-long paleoseismic record and may affect earthquake recurrence intervals within geometrically complex fault systems, including the sections of the San Andreas fault closest to metropolitan Los Angeles.

INTRODUCTION

The San Andreas fault (SAF) in central-southern California accommodates as much as 35 mm/yr (Sieh and Jahns, 1984) of the 53 mm/yr of local relative motion between the Pacific and North America plates (DeMets and Dixon, 1999). Historically, this motion has been expressed seismically by the large C.E. 1812 M_W = 7.5 Wrightwood and 1857 M_W = 7.9 Fort Tejon earthquakes (Sieh et al., 1989). Further evidence for large-magnitude earthquakes has been documented through paleoseismic studies revealing as many as 14 earthquakes averaging 3.2 m of slip per event along the central-southern SAF since C.E. 550 (Weldon et al., 2004). The spatial distribution of earthquake occurrence is not homogeneous over this time interval: seismic events have more frequently ruptured the Big Bend of the SAF, comprising the Mojave (MJ) and San Bernardino (SB) sections within 50 km of metropolitan Los Angeles (Weldon et al., 2004; Biasi and Weldon, 2009). During the past ~150 yr of relative seismic quiescence, interseismic earthquake cycle processes have continually modulated shear and Coulomb stresses on the SAF while the seismically exposed population of greater Los Angeles has grown from fewer than 10,000 to more than 10 million (Stein and Hanks, 1998).

The total stress on a seismogenic fault surface results from the cumulative effects of coseismic, postseismic, and interseismic earthquake cycle processes. Elastic models of a 200-yr-long historical earthquake catalog suggest abrupt coseismic Coulomb failure stress perturbations to 700 kPa along the SAF (King et al., 1994; Freed et al., 2007). In the decade following the 1992 M_W = 7.3 Landers and 1999 M_W = 7.1 Hector Mine earthquakes in the eastern California shear zone, postseismic deformation controlled by viscoelastic relaxation processes in the lower crust and upper mantle (Smith and Sandwell, 2006) resulted in a net 230–350 kPa increase in Coulomb failure stress (CFS) on the SB and northern Indio (IN) section of the SAF and a decrease on the MJ of 100 kPa, reducing the likelihood of failure (Freed and Lin, 2002). Except following the largest earthquakes, such as the Fort Tejon event, the contribution of postseismic deformation to the state of stress decays to apparently negligible levels within about a decade (Freed et al., 2007).

In contrast to the short time scales associated with coseismic and postseismic stress changes, interseismic stress accumulation is gradual, yet characterizes the majority of each seismic cycle, building cumulatively through the tens to hundreds of years between earthquakes and serving as the primary mechanism driving future seismicity. On-fault stress accumulates through the interseismic phase of the earthquake cycle when temporary frictional stability inhibits slip on the seismogenic fault interface, above a locking depth defined by the brittle-ductile transition zone at 15–25 km depth, causing a buildup of elastic strain within the upper crust (Fig. 1A; Savage and Burford, 1973). In the seismogenic layer this effect is modeled using the slip deficit (backslip) method (Savage, 1983), where the slip deficit rate ranges from zero for a creeping fault to the long-term

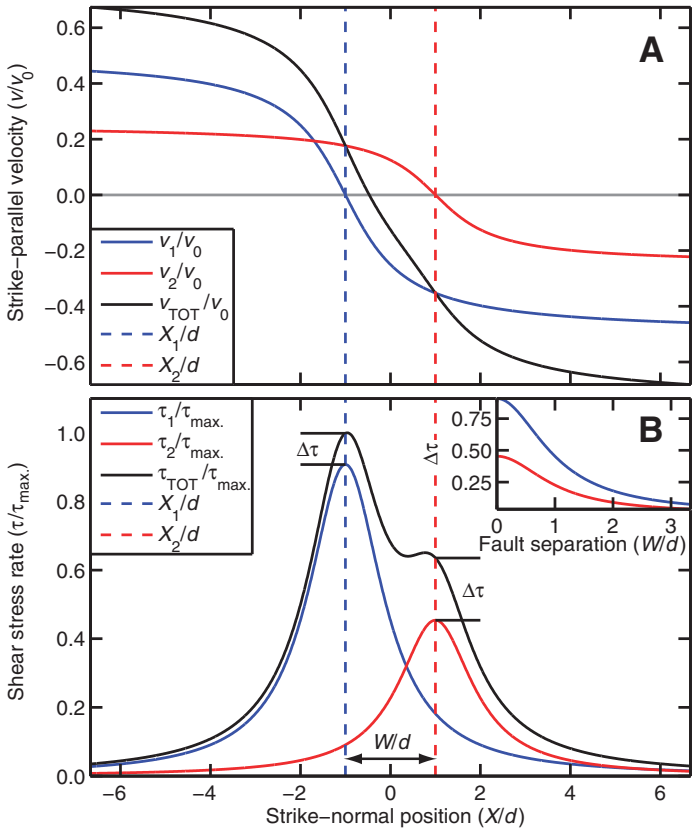

Figure 1. A: Interseismic fault-parallel surface velocities, *v*, due to slip deficit on two faults locked to depth *d* and spaced *W* = 2*d*. Slip deficit rate is v_0 on fault 1 (blue) and $v_0/2$ on fault 2 (red). Total velocity due to slip deficit on both faults is shown in black. B: Interseismic surface shear stress accumulation rates, τ. Difference between total stress accumulation rate (black line) and self-stressing rate on fault 2 (red line), Δτ, represents modulation of stress on one fault due to slip deficit on other. Inset shows decay of Δτ with fault separation, *W*/*d*.

*Current address: Department of Geosciences, Smith College, Northampton, Massachusetts 01063, USA; E-mail: jloveless@smith.edu.

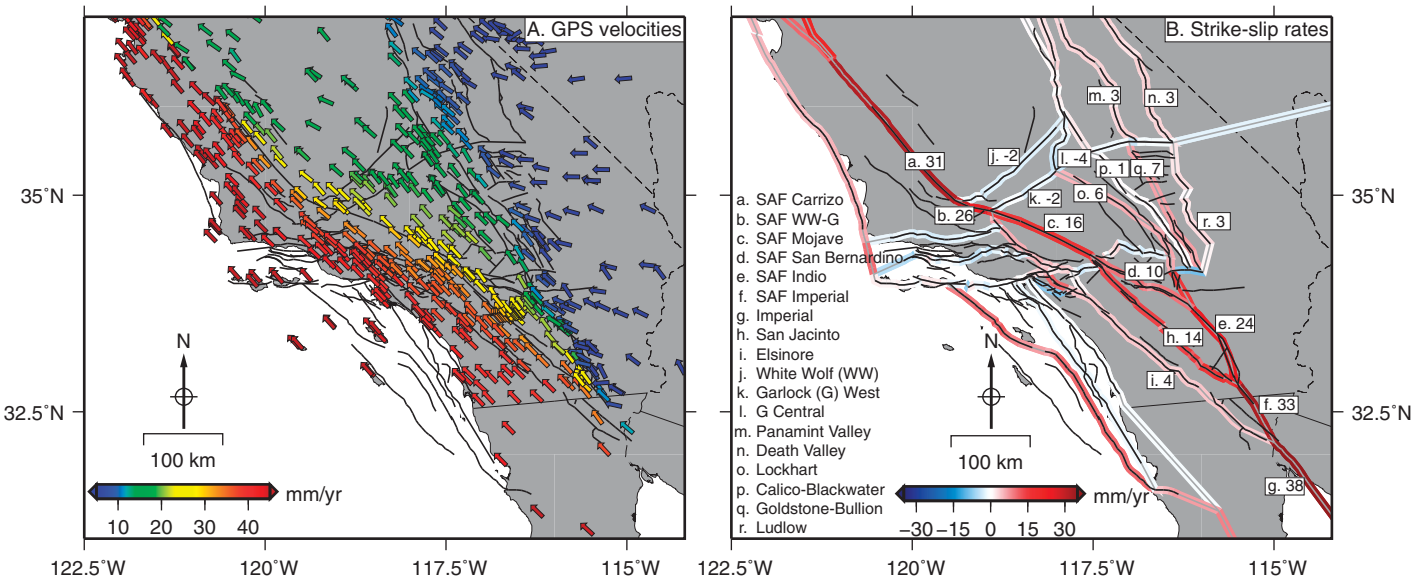

Figure 2. Block model constraints and results. A: Interseismic velocity field (McClusky et al., 2001; Shen et al., 2003; Hammond and Thatcher, 2005; Williams et al., 2006; McCaffrey et al., 2007; Plate Boundary Observatory network velocity field, http://pboweb.unavco.org) relative to stable North America. Arrow length is uniform; speed is denoted by color. GPS—global positioning system. B: Estimated strike-slip rates on block-bounding faults from our reference block model given by colored lines (right lateral is positive). Gray lines show block geometry, which is constructed by connecting faults with parameters specified by the Southern California Earthquake Center Rectilinear Community Fault Model (Plesch et al., 2007) (black lines). SAF—San Andreas fault. Selected faults are labeled with average slip rate (rounded to nearest mm/yr). Full list of slip rates is in Table DR1 (see footnote 1). Figure constructed using Generic Mapping Tools (Wessel and Smith, 1998).

fault slip rate for a locked fault. The interseismic stress accumulation rate on an isolated fault is linearly proportional to its slip deficit rate (Fig. 1B; Okada, 1992). However, stresses generated by slip deficit on one fault extend throughout the upper crust (e.g., Hetland and Hager, 2006), decaying with distance as ~1/*r* for the near-field two-dimensional case. Because of this non-local effect, the total stress accumulation on any fault segment is the sum of the contributions from all active structures within the interacting fault network (Fig. 1B).

SAN ANDREAS FAULT STRESSING RATES

To calculate current stressing rates on the southern-central SAF, we use global positioning system (GPS) measurements of interseismic deformation (Fig. 2A) (McClusky et al., 2001; Shen et al., 2003; Hammond and Thatcher, 2005; Williams et al., 2006; McCaffrey et al., 2007; Plate Boundary Observatory network velocity field, http://pboweb.unavco.org) and a three-dimensional spherical block model (see the GSA Data Repository[1]) (Meade and Loveless, 2009) to constrain kinematically consistent slip rates (Weldon and Humphreys, 1986; Minster and Jordan, 1987) on ~60,000 km^2 of fault area throughout the Southern California fault system. Block models describe the interseismic GPS velocity field as the combined effects of two processes, long-term microplate rotations and local elastic strain accumulation effects (Savage and Burford, 1973; Savage, 1983; Matsu'ura et al., 1986). Using a fault system geometry derived from the Southern California Earthquake Center Community Fault Model (Plesch et al., 2007) (Table DR1 in the Data Repository) and 1822 GPS velocities (Table DR2), we simultaneously estimate microplate rotations (yielding strike-slip rates and dip-slip [on dipping segments], or opening or closing rates [on vertical segments] on block-bounding faults), elastic strain accumulation due to interseismic locking of faults, and homogeneous strain rates within crustal microplates (McCaffrey, 2005). The block model fits the data with a mean residual velocity magnitude of 1.67 mm/yr and simultaneously satisfies far-field Pacific–North America plate motion constraints (DeMets and Dixon, 1999).

Model results show that slip on the Carrizo (CZ) section of the SAF currently accounts for as much as 60% of the 53 mm/yr of relative plate motion (DeMets and Dixon, 1999). However, the anastomosing geometry of the Southern California fault system partitions slip across multiple faults through the Big Bend region (Fig. 2B) and, as a consequence, SAF strike-slip rates vary significantly along strike: 31.2 ± 0.2 mm/yr on the CZ, 16.3 ± 0.8 mm/yr on the MJ, 10.2 ± 0.3 mm/yr on the SB, 25.4 ± 0.2 mm/yr on the IN, and 39.2 ± 0.4 mm/yr on the Imperial (IM) sections (Fig. 2B; Table DR1). The remaining 16%–74% (~10–40 mm/yr) of relative plate motion is distributed among other active faults, most significantly the San Jacinto, Elsinore, and Hosgri faults and the eastern California shear zone (McClusky et al., 2001) (Fig. 2B). The along-strike variation in SAF strike-slip rate, reaching a minimum along the SB, is consistent with late Pleistocene estimates (McGill et al., 2010).

These fault slip rates inferred from the geodetically constrained block model, interpreted as slip deficit rates, provide the basis for determining present-day interseismic stress accumulation rates on the SAF (Figs. 1 and 3; Figs. DR1–DR3). We analytically (Okada, 1992) calculate shear stress rates every ~10 km along strike at the centroid of each SAF segment, the centroid depth being defined as half the depth to which the segment is inferred to be interseismically locked. The self-stress rate, τ_{SAF}, results from slip deficit only on SAF segments, and total stress rate on the fault, τ_{TOT}, is due to slip deficit on all fault segments of the Southern California fault system. Differential stress rates, $\Delta\tau = \tau_{TOT} - \tau_{SAF}$, and the normalized percent difference, $\Delta\bar{\tau} = \Delta\tau/\tau_{SAF} \times 100$, represent the modulation of SAF stress rate due to all faults other than the SAF.

Self-shear stress rates are greatest (60–80 kPa/yr) along the southern IN and northern IM and least (11–14 kPa/yr) along the MJ and SB

[1]GSA Data Repository item 2011305, detailed description of methods, Tables DR1 and DR2, and Figures DR1–DR3, is available online at www.geosociety.org/pubs/ft2011.htm, or on request from editing@geosociety.org or Documents Secretary, GSA, P.O. Box 9140, Boulder, CO 80301, USA.

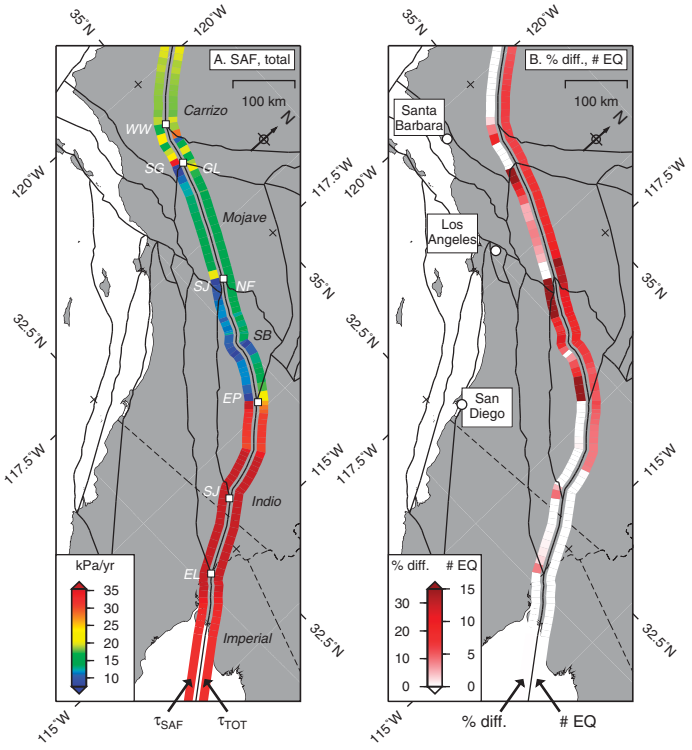

Figure 3. Interseismic shear stressing rates calculated analytically (Okada, 1992) using slip deficit rates from our kinematically consistent block model. Two quantities are plotted in each panel, one to left (southwest) and one to right (northeast) of San Andreas fault (SAF) trace, as labeled at bottom of panel. A: Self-shear stress rate due to slip deficit on SAF segments alone, τ_{SAF}, and total shear stress rate due to slip deficit on all faults, τ_{TOT}. Fault junctions are labeled in white: WW—White Wolf; GL—Garlock; SG—San Gabriel; SJ—San Jacinto; NF—North Frontal; EP—Eureka Peak; EL—Elsinore. Junctions bound labeled sections of SAF: SB—San Bernardino. B: Percent difference between total and self-stress, normalized by self-stress, $\Delta\bar{\tau}$ (% diff.), and mean number of paleoseismic earthquakes on each model segment (# EQ), from rupture models of Biasi and Weldon (2009). Figure constructed using Generic Mapping Tools (Wessel and Smith, 1998).

(Fig. 3A), where fault slip deficit rates are lowest. Slip deficit rates are highest along the CZ and IM (31.5 and 38 mm/yr, respectively) (Fig. 2B), but τ_{SAF} values are moderate (~18–32 kPa/yr) due to greater locking depths along the CZ (20–25 km) and IM (15 km) than along the IN (5.0–7.5 km) (Table DR1). Total stress rates, τ_{TOT}, show a spatial distribution similar to τ_{SAF}, but are significantly higher (~14–17 kPa/yr) along the MJ and SB (Fig. 2B).

Stress rate modulation, $\Delta\bar{\tau}$, shows peaks at fault junctions, resulting from singularities at fault triple junctions that are incompletely cancelled by adjacent segments in the fault geometry subset considered in calculating τ_{SAF}. These artifacts persist for only ~10 km, and we focus on values away from junctions, which reach +38% along the MJ and SB (Fig. 3B). Stress increases (positive $\Delta\bar{\tau}$) result from the cumulative effect of the interseismic stress fields generated by the nearby White Wolf, Garlock, San Gabriel, North Frontal, Eureka Peak, and San Jacinto faults, as well as the eastern California shear zone. Assuming a 45° north-dipping San Gorgonio Pass fault segment, $\Delta\bar{\tau}$ along SB is decreased by an average of 8.7% relative to the vertically dipping reference model, primarily due to three negative $\Delta\bar{\tau}$ dipping segments; the overall SB stress increases are similar. Except at fault junctions, $\Delta\bar{\tau}$ is negligible along the CZ, IN, and IM, where the SAF is relatively isolated from neighboring faults.

DISCUSSION

A consequence of the increased shear stress rates is that interseismic fault system interactions may reduce the time required to accumulate the stresses necessary for seismic failure on the MJ and SB relative to the time predicted by τ_{SAF} alone. Annual $\Delta\tau$ along the SB (mean 2.8 kPa/yr, maximum 6.8 kPa/yr) is ~2 orders of magnitude smaller than the coseismic and postseismic stress changes induced by the recent Landers and Hector Mine eastern California shear zone earthquakes (Freed and Lin, 2002). However, the cumulative effect of interseismic shear stress modulation reaches a maximum of 1 MPa when integrated over the ~150 yr since the 1857 Fort Tejon earthquake. This value is ~3 times the maximum (~300 kPa) shear stress induced by the Landers earthquake on the SB (King et al., 1994). Thus, in terms of stress perturbations that may trigger earthquakes and control long-term seismicity patterns, interseismic stress modulation is of a magnitude similar to that of coseismic and postseismic sources along the SB and, more important, continues to influence this section long after the earthquake-related stress changes have decayed to negligible levels, though ongoing postseismic deformation occurring at a rate below the current detection limits of GPS (Freed et al., 2007) may be considered a part of the nominally interseismic period. The CFS ($= \tau - \mu\sigma_n$, where μ is the effective coefficient of friction and σ_n is normal stress) on the MJ was reduced as much as 50 kPa coseismically due to the Landers earthquake (King et al., 1994; Freed and Lin, 2002) and as much as 100 kPa by postseismic deformation following the Landers and Hector Mine events (Freed and Lin, 2002). In contrast, interseismic fault system interactions have induced a positive CFS change of as much as 540 kPa during the post–Fort Tejon epoch ($CFS_{TOT} - CFS_{SAF} \approx 3.6$ kPa/yr maximum; 1.8 kPa/yr mean). This outweighs the negative changes caused by recent eastern California shear zone earthquakes by 440–490 kPa and suggests that interseismic fault system interactions over the past 150 yr have been the largest magnitude off-SAF source of stress with the potential to reduce earthquake recurrence intervals.

Assuming uniform fault strength along strike and homogeneous coseismic stress drops, estimated recurrence intervals of large earthquakes on the entire SAF based on τ_{SAF} or τ_{TOT} would suggest that earthquakes occur more frequently on the high-stress-rate CZ, IN, and IM sections than along the MJ and SB sections. However, this simple idealization is inconsistent with paleoseismic data, which suggest that Big Bend sections have ruptured in at least as many earthquakes as the CZ (Grant Ludwig et al., 2010) and more than the IN and IM (Weldon et al., 2004; Biasi and Weldon, 2009). Based on data compiled at paleoseismic sites along the SAF between the CZ and IN, admissible rupture models (Weldon et al., 2004; Biasi and Weldon, 2009) support the occurrence of 12–26 earthquakes in the past 1500 yr. For these models, we count the number of inferred events that involved each ~10-km-long segment of the SAF used in our stress rate calculations (Fig. 3B). Though the models vary in number of events and rupture extents due to uncertainties in stratigraphic offset and age measurements and correlation of data from site to site (Biasi and Weldon, 2009), those that have been published (Weldon et al., 2004; Biasi and Weldon, 2009) show a greater number of inferred events rupturing the MJ and SB than elsewhere along strike, where $\Delta\bar{\tau}$ is generally positive (Fig. 3B). Interseismic stress modulation may, however, be modified by subsequent coseismic and postseismic effects, such as the decrease in failure stress induced on the MJ by eastern California shear zone earthquakes (King et al., 1994). Therefore, any relationship between $\Delta\bar{\tau}$ and earthquake recurrence interval may only be relevant during a single interseismic phase. Regardless, SAF earthquake recurrence intervals estimated from τ_{SAF}, assuming uniform fault strength and coseismic stress drop, may be overestimated.

ACKNOWLEDGMENTS

We thank James Dolan and an anonymous referee for helpful reviews and Michele Cooke for reviewing a previous version. This research was supported by

funding from Harvard University and the Southern California Earthquake Center (SCEC). SCEC is funded by National Science Foundation Cooperative Agreement EAR-0106924 and U.S. Geological Survey Cooperative Agreement 02HQAG0008. The SCEC contribution number for this paper is 1499.

REFERENCES CITED

Biasi, G.P., and Weldon, R.J., 2009, San Andreas fault rupture scenarios from multiple paleoseismic records: Stringing pearls: Seismological Society of America Bulletin, v. 99, p. 471–498, doi:10.1785/0120080287.

DeMets, C., and Dixon, T.H., 1999, New kinematic models for Pacific–North America motion from 3 Ma to present, I: Evidence for steady motion and biases in the NUVEL-1A model: Geophysical Research Letters, v. 26, p. 1921–1924, doi:10.1029/1999GL900405.

Freed, A.M., and Lin, J., 2002, Accelerated stress buildup on the southern San Andreas fault and surrounding regions caused by Mojave Desert earthquakes: Geology, v. 30, p. 571–574, doi:10.1130/0091-7613(2002)030<0571:ASBOTS>2.0.CO;2.

Freed, A.M., Ali, S.T., and Bürgmann, R., 2007, Evolution of stress in southern California for the past 200 years from coseismic, postseismic and interseismic stress changes: Geophysical Journal International, v. 169, p. 1164–1179, doi:10.1111/j.1365-246X.2007.03391.x.

Grant Ludwig, L., Akçiz, S.O., Noriega, G.R., Zielke, O., and Arrowsmith, J.R., 2010, Climate-modulated channel incision and rupture history of the San Andreas fault in the Carrizo Plain: Science, v. 327, p. 1117–1119, doi:10.1126/science.1182837.

Hammond, W.C., and Thatcher, W., 2005, Northwest Basin and Range tectonic deformation observed with the Global Positioning System, 1999–2003: Journal of Geophysical Research, v. 110, B10405, doi:10.1029/2005JB003678.

Hetland, E.A., and Hager, B.H., 2006, Interseismic strain accumulation: Spin-up, cycle invariance, and irregular rupture sequences: Geochemistry Geophysics Geosystems, v. 7, Q05004, doi:10.1029/2005GC001087.

King, G.C.P., Stein, R.S., and Lin, J., 1994, Static stress changes and the triggering of earthquakes: Seismological Society of America Bulletin, v. 84, p. 935–953.

Matsu'ura, M., Jackson, D.D., and Cheng, A., 1986, Dislocation model for aseismic crustal deformation at Hollister, California: Journal of Geophysical Research, v. 91, no. B12, p. 2661–2674, doi:10.1029/JB091iB12p12661.

McCaffrey, R., 2005, Block kinematics of the Pacific–North America plate boundary in the southwestern United States from inversion of GPS, seismological, and geologic data: Journal of Geophysical Research, v. 110, B07401, doi:10.1029/2004JB003307.

McCaffrey, R., Qamar, A.I., King, R.W., Wells, R., Khazaradze, G., Williams, C.A., Stevens, C.W., Vollick, J.J., and Zwick, P.C., 2007, Fault locking, block rotation and crustal deformation in the Pacific Northwest: Geophysical Journal International, v. 169, p. 1315–1340, doi:10.1111/j.1365-246X.2007.03371.x.

McClusky, S.C., Bjornstad, S.C., Hager, B.H., King, R.W., Meade, B.J., Miller, M.M., Monastero, F.C., and Souter, B.J., 2001, Present day kinematics of the Eastern California Shear Zone from a geodetically constrained block model: Geophysical Research Letters, v. 28, p. 3369–3372, doi:10.1029/2001GL013091.

McGill, S., Weldon, R., and Owen, L., 2010, Latest Pleistocene slip rates along the San Bernardino strand of the San Andreas fault: Geological Society of America Abstracts with Programs, v. 42, no. 4, p. 69.

Meade, B.J., and Loveless, J.P., 2009, Block modeling with connected fault network geometries and a linear elastic coupling estimator in spherical coordinates: Seismological Society of America Bulletin, v. 99, p. 3124–3139, doi:10.1785/0120090088.

Minster, J.B., and Jordan, T.H., 1987, Vector constraints on western United States deformation from space geodesy, neotectonics, and plate motions: Journal of Geophysical Research, v. 92, p. 4798–4804, doi:10.1029/JB092iB06p04798.

Okada, Y., 1992, Internal deformation due to shear and tensile faults in a half-space: Seismological Society of America Bulletin, v. 82, p. 1018–1040.

Plesch, A., and 27 others, 2007, Community Fault Model (CFM) for southern California: Seismological Society of America Bulletin, v. 97, p. 1793–1802, doi:10.1785/0120050211.

Savage, J.C., 1983, A dislocation model of strain accumulation and release at a subduction zone: Journal of Geophysical Research, v. 88, p. 4984–4996, doi:10.1029/JB088iB06p04984.

Savage, J.C., and Burford, R.O., 1973, Geodetic determination of relative plate motion in central California: Journal of Geophysical Research, v. 78, p. 832–845, doi:10.1029/JB078i005p00832.

Shen, Z.K., Agnew, D.C., King, R.W., Dong, D., Herring, T.A., Wang, M., Johnson, H., Anderson, G., Nikolaidis, R., van Domselaar, M., Hudnut, K.W., and Jackson, D.D., 2003, SCEC crustal motion map, version 3.0: http://epicenter.usc.edu/cmm3.

Sieh, K.E., and Jahns, R.H., 1984, Holocene activity of the San Andreas fault at Wallace Creek, California: Geological Society of America Bulletin, v. 95, p. 883–896, doi:10.1130/0016-7606(1984)95<883:HAOTSA>2.0.CO;2.

Sieh, K., Stuiver, M., and Brillinger, D., 1989, A more precise chronology of earthquakes produced by the San Andreas fault in southern California: Journal of Geophysical Research, v. 94, p. 603–623, doi:10.1029/JB094iB01p00603.

Smith, B.R., and Sandwell, D.T., 2006, A model of the earthquake cycle along the San Andreas fault system for the past 1000 years: Journal of Geophysical Research, v. 111, B01405, doi:10.1029/2005JB003703.

Stein, R.S., and Hanks, T.C., 1998, M >= 6 earthquakes in southern California during the twentieth century: No evidence for a seismicity or moment deficit: Seismological Society of America Bulletin, v. 88, p. 635–652.

Weldon, R., and Humphreys, E., 1986, A kinematic model of southern California: Tectonics, v. 5, p. 33–48, doi:10.1029/TC005i001p00033.

Weldon, R., Scharer, K., Fumal, T., and Biasi, G., 2004, Wrightwood and the earthquake cycle: What a long recurrence record tells us about how faults work: GSA Today, v. 14, no. 9, p. 4–10, doi:10.1130/1052-5173(2004)014<4:WATECW>2.0.CO;2.

Wessel, P., and Smith, W.H.F., 1998, New, improved version of Generic Mapping Tools: Eos (Transactions, American Geophysical Union), v. 79, p. 579, doi:10.1029/98EO00426.

Williams, T.B., Kelsey, H.M., and Freymueller, J.T., 2006, GPS-derived strain in northwestern California: Termination of the San Andreas fault system and convergence of the Sierra Nevada–Great Valley block contribute to southern Cascadia forearc contraction: Tectonophysics, v. 413, p. 171–184, doi:10.1016/j.tecto.2005.10.047.

Manuscript received 1 March 2011
Revised manuscript received 6 June 2011
Manuscript accepted 17 June 2011

Printed in USA